International Journal of Bifurcation and Chaos, Vol. 27, No. 2 (2017) 1730008 (19 pages)

DOI: 10.1142/S0218127417300087

Detecting Hidden Chaotic Regions and Complex Dynamics in the Self-Exciting Homopolar Disc Dynamo

Zhouchao Wei
School of Mathematics and Physics,
China University of Geosciences,
Wuhan 430074, P. R. China

Guangxi Colleges and Universities Key Laboratory
of Complex System Optimization and Big Data Processing,
Yulin Normal University, Yulin 537000, P. R. China

Mathematical Institute, University of Oxford,
Oxford, OX2 6GG, England

College of Mechanical Engineering,
Beijing University of Technology,
Beijing 100124, P. R. China

Zhouchao.Wei@maths.ox.ac.uk
weizhouchao@163.com

Irene Moroz
Mathematical Institute, University of Oxford,
Oxford, OX2 6GG, England

Julien Clinton Sprott
Department of Physics, University of Wisconsin,
Madison, WI 53706, USA

Zhen Wang
Department of Applied Sciences,
Xijing University, Xi'an 710123, P. R. China

Wei Zhang*
College of Mechanical Engineering,
Beijing University of Technology,
Beijing 100124, P. R. China
sandyzhang0@yahoo.com

Received August 12, 2016; Revised October 12, 2016

In 1979, Moffatt pointed out that the conventional treatment of the simplest self-exciting homopolar disc dynamo has inconsistencies because of the neglect of induced azimuthal eddy currents, which can be resolved by introducing a segmented disc dynamo. Here we return to the simple dynamo system proposed by Moffatt, and demonstrate previously unknown hidden chaotic attractors. Then we study multistability and coexistence of three types of attractors in

*Author for correspondence

the autonomous dynamo system in three dimensions: equilibrium points, limit cycles and hidden chaotic attractors. In addition, the existence of two homoclinic orbits is proved rigorously by the generalized Melnikov method. Finally, by using Poincaré compactification of polynomial vector fields in three dimensions, the dynamics near infinity of singularities is obtained.

Keywords: Homopolar disc dynamo; hidden attractor; multistability and coexistence; homoclinic orbit; dynamics at infinity.

1. Introduction

To the extent that they have been known to exist, complex dynamical behaviors with stable equilibria have mostly been considered to be impossible. In this connection it is interesting to recall, for instance, how the presence of an unstable equilibrium point plays an essential role in Shilnikov's famous criterion for the onset of chaos [Shilnikov, 1965; Silva, 1993]. From a computational point of view, this allows one to use numerical methods, in which after transients have decayed, a trajectory, starting from a point of an unstable manifold in the neighborhood of an unstable equilibrium, reaches an attractor and identifies it.

The study of chaotic systems is an important and yet difficult task in the theory of nonlinear dynamical systems. There is a long history for the study of related topics. However, the concept of a "hidden attractor" was introduced in the mid-20th century in connection with discussions among leading scientists of the field about problems associated with polynomial systems, embedded oscillations, global stability, etc. [Leonov & Kuznetsov, 2013]. The problem of analyzing hidden periodic oscillations first arose in the second part of Hilbert's 16th problem, which considered the number and mutual disposition of limit cycles in two-dimensional polynomial systems [Hilbert, 1901]. Hidden oscillations appear naturally in systems without equilibria, describing various mechanical and electromechanical models with rotation, and electrical circuits with cylindrical phase space [Sommerfeld, 1902; Blekhman *et al.*, 2007; Eckert & Sommerfeld, 2013].

During the last few years, more complex hidden attractors, in particular hidden chaos, have been studied by many researchers. For example, hidden chaotic attractors are attractors in systems with no equilibria or with only one stable equilibrium (a special case of the multistability: coexistence of attractors in multistable systems). A rapidly growing number of studies have been published in which hidden chaotic attractors are shown to exist in the absence of any form of equilibrium point or in the presence of only stable equilibrium points (see, e.g. [Wei, 2011; Wei & Yang, 2011, 2012; Wang *et al.*, 2012; Wang & Chen, 2012, 2013; Jafari *et al.*, 2013; Wei *et al.*, 2015a; Wei *et al.*, 2015b]). Therefore, systems that exhibit complex nonlinear dynamical behavior do not need to display an unstable equilibrium. In addition, multistability can be inconvenient in various practical applications [Leonov *et al.*, 2015a]. From a computational perspective, it is natural to suggest the classification of attractors in [Leonov *et al.*, 2012], which is based on the simplicity of finding their basins of attraction in phase space. Hidden attractors arise in connection with various fundamental problems and applied models. Hidden periodic oscillations and hidden chaotic attractors have been studied in applied models [Andrievsky *et al.*, 2013; Leonov *et al.*, 2014; Zhusubaliyev *et al.*, 2015; Leonov *et al.*, 2015b; Kuznetsov *et al.*, 2015; Kuznetsov *et al.*, 2016; Wei *et al.*, 2016; Kiseleva *et al.*, 2016].

The present interest in hidden attractors motivates us to ask whether chaotic states can be observed in the homopolar dynamo without unstable equilibria. The purpose of the present paper is to examine and study the hidden chaos, homoclinic orbits and dynamics near infinity in a self-exciting homopolar disc dynamo, proposed by Moffatt in 1979 [Moffatt, 1979], which was not yet then completely well understood. The possibility of the existence of hidden chaotic attractors in the disc dynamo is confirmed. We also discuss the mechanisms responsible for maintaining the oscillatory dynamics in the homopolar disc dynamo and provide an overview of the distribution in 2D parameter space. What leads to the generation of hidden attractors is demonstrated by two unstable periodic

solutions from a Hopf bifurcation near the stable equilibria. In addition, by using the generalized Melnikov method, the existence of homoclinic orbits is proved. Finally, we also give a complete description of its dynamics on the Poincaré sphere at infinity by using the Poincaré compactification of a polynomial vector field in R^3, showing that there are indeed orbits which escape to, or come from, infinity, instead of going towards the attractors.

2. Description of the Self-Exciting Homopolar Disc Dynamo and Related Problems

The self-exciting homopolar dynamo is one of the simplest models of the self-excitation of a magnetic field by moving conductors. It is often used to illustrate the dynamo action that is thought to lie behind the generation of the magnetic fields of the Earth, the Sun and other cosmic bodies [Moffatt, 1978; Beck *et al.*, 1996]. In its simplest form, originally considered by Bullard [1955], the dynamo consists of a solid metal disc which rotates about an axis, perpendicular to the disc, and a wire twisted around it, and connected through sliding contacts to the rim and the axis of the disc.

Model dynamos have been extensively investigated in the past as an aid to understanding the generation of magnetic fields and their reversals in astrophysical bodies. In 1979, Moffatt pointed out that the conventional treatment of the simplest such model [Moffatt, 1979], the self-exciting Bullard dynamo [Knobloch, 1981; Hide *et al.*, 1996; Moroz *et al.*, 1998; Priede & Avalos-Zúñiga, 2013], was not self-consistent because it neglected the currents associated with the radial diffusion of the magnetic field, and so introduced a segmented disc dynamo in which this effect could be included in a simple way. This dynamo is described by the following system of nondimensionalized ordinary differential equations:

$$\begin{cases} \dot{x} = r(y - x), \\ \dot{y} = mx - (1 + m)y + xz, \\ \dot{z} = g[1 + mx^2 - (1 + m)xy]. \end{cases} \tag{1}$$

Here $x(t)$ and $y(t)$ denote the magnetic fluxes due to radial and azimuthal current distributions respectively, $z(t)$ is the angular velocity of the disc, the dot denoting differentiation with respect to time, g measures the applied torque, and r and m are positive constants that depend on the electrical properties of the circuit.

System (1) has the equilibrium states $E_{1,2} = (\pm 1, \pm 1, 1)$, which exist for any parameter values. It is easy to see the invariance of (1) under the transformation $(x, y, z) \to (-x, -y, z)$, namely the system has reflected symmetry around the z-axis. Therefore, we only consider the dynamics of E_1. The Jacobian matrix of system (1), evaluated at the equilibrium E_1 is

$$J(E_1) = \begin{pmatrix} -r & r & 0 \\ 1 + m & -1 - m & 1 \\ g(-1 + m) & g(-1 - m) & 0 \end{pmatrix}$$

and its corresponding characteristic equation is

$$2gr + (g + gm)\lambda + (1 + m + r)\lambda^2 + \lambda^3 = 0. \tag{2}$$

According to the Routh–Hurwitz criterion since r, g, m are all real positive parameters, the characteristic polynomial (2) has three roots with negative real parts under the following conditions:

$$m \geq 1 \quad \text{or} \quad m < 1, \quad r < \frac{(m + 1)^2}{1 - m}. \tag{3}$$

Note that the negative characteristic value corresponds to the contraction direction while the positive real parts of the conjugate pair of complex characteristic values correspond to the prolongation direction in the Smale map, if it exists. Based on the above discussions, the following property can be easily verified.

Proposition 2.1. *Let $r > 0$, $g > 0$, $m > 0$ and $r_0 = \frac{(m+1)^2}{1-m}$. Then, system (1) has two equilibria*:

$$E_{1,2}(\pm 1, \pm 1, 1).$$

Furthermore,

(i) *if $m \geq 1$ or $m < 1$, $r < r_0$, then the equilibria $E_{1,2}$ are locally asymptotically stable nodes, or node-foci, at each of which the stable manifolds $W^s(E_{1,2})$ are three-dimensional*;

(ii) *if $m < 1$, $r > r_0$, then the equilibria $E_{1,2}$ are saddle-foci, at each of which the stable manifold $W^s(E_{1,2})$ is one-dimensional and the unstable manifold $W^u(E_{1,2})$ is two-dimensional.*

By combining Proposition 2.1(i)–(ii) and the eigenvalue structures from (2) of the linearized system of system (1) at their corresponding equilibria,

as discussed above, one arrives at the following result:

Proposition 2.2. *Denoting* $r_0 = \frac{(m+1)^2}{1-m}$, *system* (*1*) *with parameters*

$$(r, g, m) \in \Omega_1 = \{(r, g, m) \,|\, g > 0, m \geq 1 \text{ or } g > 0, m < 1, 0 < r < r_0\}$$

is not diffeomorphic to, and so is not topologically equivalent to, any known three-dimensional autonomous chaotic system in the form of (*1*) *with parameters*

$$(r, g, m) \in \Omega_2 = \{(r, g, m) \,|\, g > 0, m < 1, r > r_0\}.$$

Compare this with the term "hidden oscillations", introduced in connection with the classic discussion of Hilbert–Kolmogorov type problems [Hilbert, 1901]. The questions include (i) what are the possible mechanisms of birth for hidden chaotic attractors, (ii) do the associated bifurcation scenarios display particular features, and (iii) do systems of this type arise in connection with concrete practical problems [Leonov & Kuznetsov, 2013].

Until a few years ago, chaotic systems with only stable equilibria were commonly rejected as impossible. Therefore, Moffatt made the following statement about system (1) "*When* $r < (1 - m)^{-1}(l + m)^2$, *it seems probable that all trajectories tend to one of the two equilibrium points*" [Moffatt, 1979]. However, for parameters $(r, m, g) = (10, 0.75, 20)$ and initial values $(0.3, 2.9, 0.1)$, it is known analytically that system (1) has two stable equilibria with 3D stable and no unstable manifolds. Numerical simulations show trajectories from the initial data given in Fig. 1. Basins of attraction for system (1) with only stable equilibria versus selected parameters and initial values are shown in Fig. 2. The plots show a cross-section in the planes which contain the two stable equilibrium points, indicated in black and their corresponding basins of attraction in green and yellow with the basin for the strange attractor in light blue. The black lines in the blue region are a cross-section of the strange attractor.

In addition, Fig. 4 shows the distribution of dynamical behaviors for system (1) in the (r, m)-plane. As previously noted, g does not affect the stability of two equilibria, and will be set 20 in Fig. 3. The red regions represent parameter sets that produce chaotic solutions. The green regions represent the stable regions, and the light blue regions represent periodic behavior. Note, however, that several regions display coexisting attracting states of different types.

2.1. *Coexistence of stable equilibria and hidden attractor*

In order to study the effect of the parameter r on the dynamics of the 3D system, we fix the parameters $m = 0.75$, $g = 20$, and vary r in the interval $8 \leq r \leq 15$. In particular, we find there are no unstable equilibria in the region $r \in [8, 12.25)$.

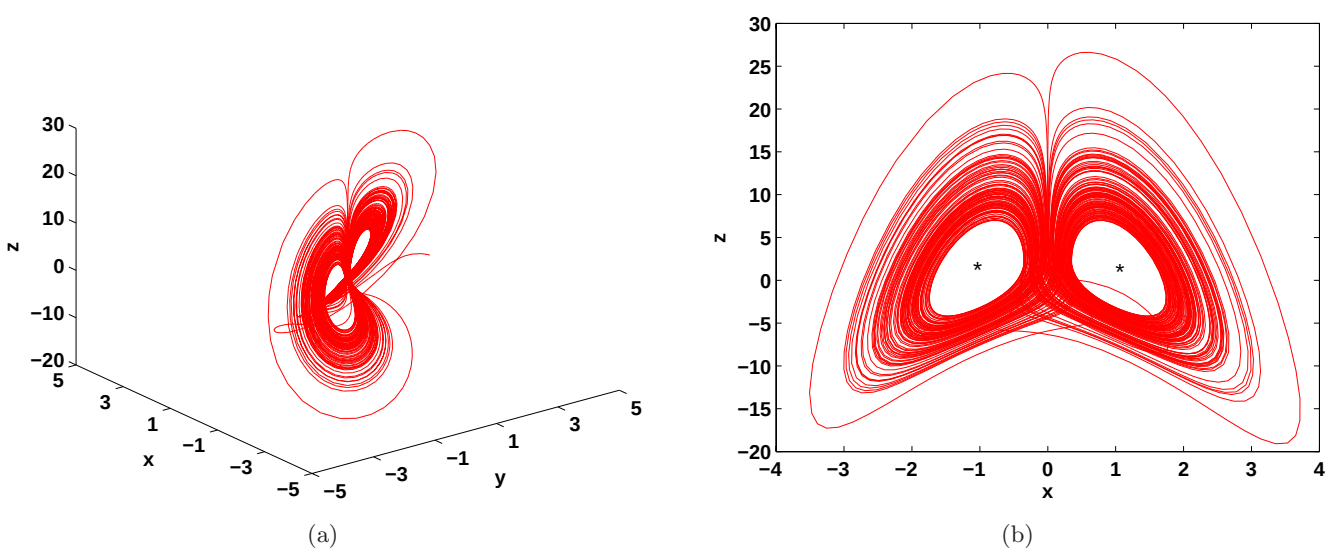

(a) (b)

Fig. 1. Phase diagram of the system (1) with only stable equilibria when parameters $(a, m, g) = (10, 0.75, 20)$ and initial values $(0.3, 2.9, 0.1)$.

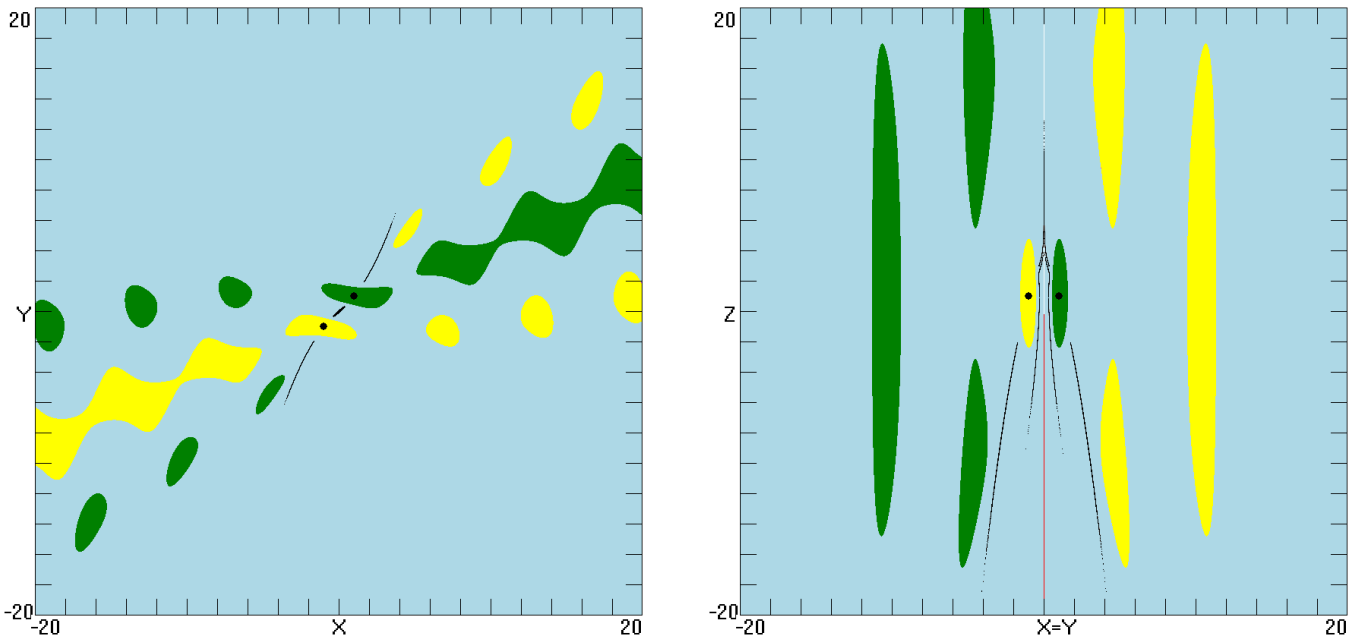

(a) (b)

Fig. 2. Basins of attraction for the system (1) with only stable equilibria for parameters $(r, m, g) = (10, 0.75, 20)$ and initial values $(0.3, 2.9, 0.1)$ on (a) $z = 1$ and (b) $x = y$.

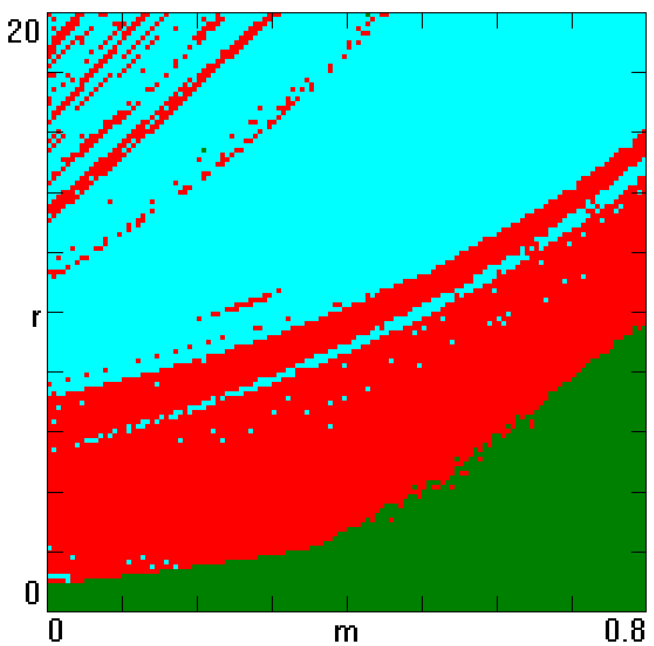

Fig. 3. Regions of various dynamical behaviors in system (1) as a function of the bifurcation parameters r and m. The chaotic regions are shown in red, the stable regions are shown in green, and the periodic regions are shown in blue.

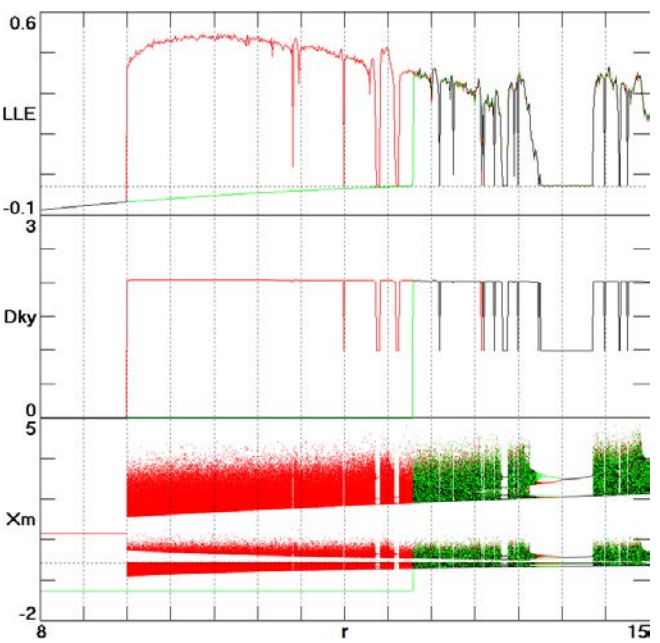

Fig. 4. The largest Lyapunov exponents, Kaplan–Yorke dimensions, and bifurcation diagrams of system (1) versus parameter $r \in [8, 15)$ and two sets of initial points: initial values $(0.3, 2.9, 0.1)$ (red); initial values $(1, 1, 1.75)$ (green).

It is well known that certain dynamical properties of system (1) can be analyzed through both its Lyapunov exponent spectrum and bifurcation diagrams. Bifurcation diagrams obtained by scanning the interval around the $r \in [8, 15]$ with different initial conditions ((0.3, 2.9, 0.1) (red), resp., (1, 1, 1.75) (green)). At both ends, the bifurcation diagram displays chaotic dynamics (Fig. 4, bottom picture). The red shows larger regions of parameter space in which the system (1) has hidden chaotic dynamics. The largest Lyapunov exponent for $r \in [8, 15]$ using initial values (0.3, 2.9, 0.1) is shown in red in Fig. 4 (top picture), while that for initial conditions (1, 1, 1.75) is shown in green. We observe that for $r \in [9, 12.151]$, in which equilibria $E_{1,2}$ are stable, the behavior of system (1) is completely different for the two sets of initial conditions. The Kaplan–Yorke dimension (Dky) is plotted in Fig. 4 (middle picture) [Kuznetsov *et al.*, 2014; Leonov *et al.*, 2015a; Kuznetsov, 2016]. These features show the region of hysteresis and coexisting attractors.

Related open problems about ergodicity or mixing property of the Moffatt's system (1) would be to understand the properties of hidden chaos. The LEs are calculated using Wolf's method to run the orbit for a time of 4e7 using a fourth-order Runge–Kutta integrator with an adaptive step size (which usually takes about a day on a fast PC), and we check that all the quoted digits are reproduced for at least two arbitrarily chosen initial conditions in the basin of the attractor.

3. Study of Hidden Attractors from a Simple Linear Transformation

When coexisting attractors occur in a system, engineers and scientists are usually interested in obtaining the basins of attraction of the different attracting sets, defined as the set of initial points whose trajectories converge on the given attractor. In Sec. 3.1, we find that the behavior not only depends on the value of the system parameters but also on the initial conditions.

Under the following linear transformation

$$\begin{cases} x_1 = x - k_1, \\ y_1 = y - k_2, \\ z_1 = z - k_3, \end{cases}$$

system (1) becomes

$$\begin{cases} \dot{x}_1 = r(y_1 - x_1) + r(k_2 - k_1), \\ \dot{y}_1 = m(x_1 + k_1) - (1 + m)(y_1 + k_2) \\ \qquad + (z_1 - k_3)(x_1 + k_1), \\ \dot{z}_1 = g[1 + m(x_1 + k_1)^2 \\ \qquad - (1 + m)(x_1 + k_1)(y_1 + k_2)], \end{cases} \tag{4}$$

where $k_i \neq 0$ $(i = 1, 2, 3)$ are three constants. The Hartman–Grobman theorem states that the local behavior of an autonomous dynamical system in the neighborhood of an hyperbolic equilibrium is qualitatively the same as (i.e. topologically equivalent to) the behavior of its linearization near this equilibrium. No matter how the values $k_i \neq 0$ $(i = 1, 2, 3)$ change, the characteristic equations of system (4) and system (1) have same eigenvalues at corresponding equilibria.

We now consider the impact of translating the coordinates when the initial conditions $(x_0, y_0, z_0) = (1, 1, 1.75)$ and system parameters $r = 10$, $m = 0.75$, $g = 20$ do not change. In particular, when $k_i \neq 0$ $(i = 1, 2, 3)$ the system (4) [which is topologically equivalent to system (1)] has only two stable equilibria and has no chaotic dynamics. This can be confirmed by calculating the Lyapunov exponents to give: $L_1 = -0.0332$, $L_2 = -0.0332$, $L_3 = -11.6836$. We next give some numerical results to show the dynamics of the system (4).

Although system (4) has only two hyperbolic stable equilibria, the transformed system is chaotic globally for certain parameter k_i $(i = 1, 2, 3)$ choices. It is apparent that system (1) with two stable equilibria that were once thought to be unusual, may in fact, be rather common, and belongs to the class of chaotic systems with hidden attractors. It is worth noting that coexisting attractors and the fractal basins may not be observed in a controlled experiment where system parameters are smoothly varied. In such instances the initial condition and coordinate transformation for each parameter value are the final condition (or state) for the previous parameter and the trajectories are therefore locked onto only one of the attracting sets.

Figure 5 shows the dynamical regions in the 2D parameter spaces (k_1–k_2) and (k_1–k_3) of system (4) for $k_i \in [-10, 10]$ $(i = 1, 2, 3)$. The ten distinct green regions in the (k_1–k_2)-plane correspond to

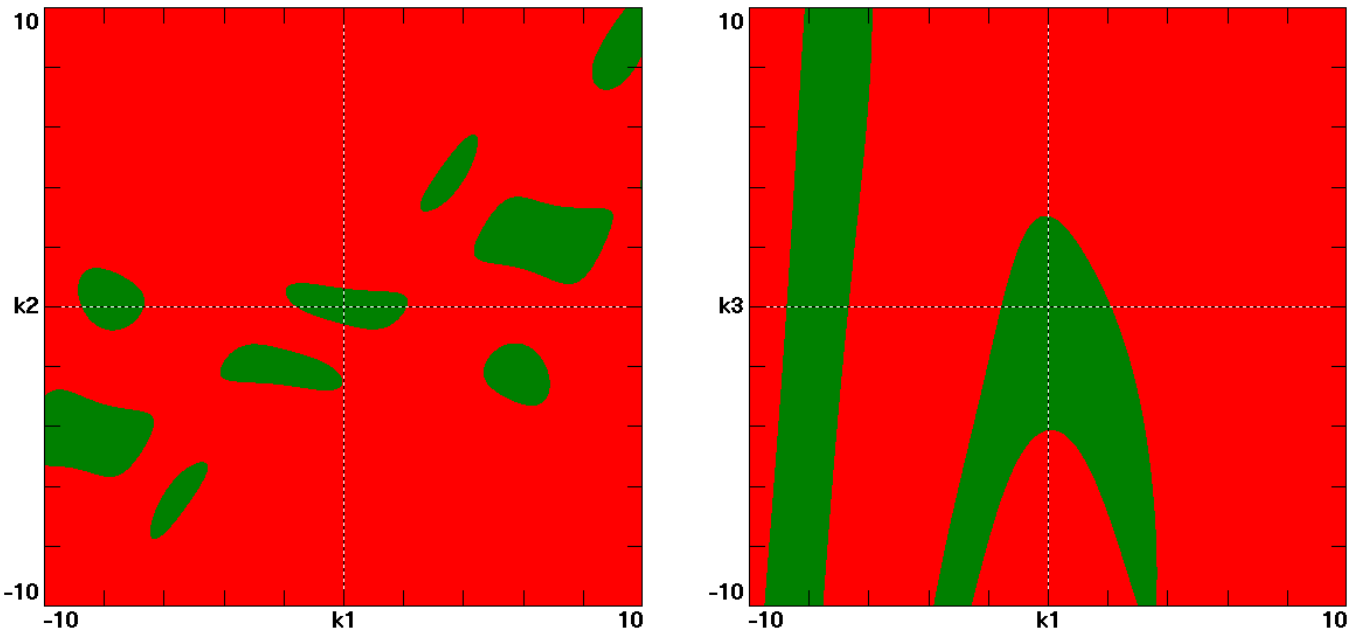

Fig. 5. Dynamical regions of system (4) with initial values $(1, 1, 1.75)$ (left and right dynamics correspond to $(k_1, k_2) \in [-10, 10] \times [-10, 10]$ and $(k_1, k_3) \in [-10, 10] \times [-10, 10]$, respectively). Green regions mean stable steady states, while red regions mean hidden chaotic attractors.

stable steady states, while the red regions correspond to hidden chaotic attractors. In the k_1–k_3-plane, there are only two distinct green regions. For each point in this plot, it was necessary to search for initial conditions that give bounded solutions and then to estimate the largest Lyapunov exponent for each point. The criterion used was to assume that Lyapunov exponents in the range $(-0.001, 0.001)$ are periodic (limit cycles), while those that are more negative correspond to stable equilibria (point attractors, shown in green), and those that are more positive correspond to chaotic (hidden attractors, shown in red).

4. Study of Hidden Attractors from Hopf Bifurcation

As far as we know, the simplest way to create a periodic orbit is through a Hopf bifurcation. The analysis of the codimension-one Hopf bifurcation about an equilibrium, using the center manifold theorem is presented in [Kuznetsov, 2014].

4.1. *An outline of the Hopf bifurcation methods*

Suppose that the characteristic equation of system (1) has a pair of pure imaginary roots $\pm i\omega$ ($\omega \in \mathbb{R}^+$). For convenience, we take $k = m + 1$. It is easy to show that when

$$r = r_0 = \frac{(m+1)^2}{1-m} = \frac{k^2}{2-k},$$

Eq. (2) yields

$$\lambda_1 = \frac{2k}{k-2} < 0, \quad \lambda_{2,3} = \pm\sqrt{gk}i,$$

where $1 < k < 2$ $(0 < m < 1)$. Summarizing, we have the following proposition:

Proposition 4.1. *Define*

$$T = \left\{ (r, g, k) \,|\, r > 0, g > 0, \right.$$
$$\left. r = r_0 = \frac{k^2}{2-k}, 1 < k < 2 \right\},$$

then the Jacobian matrix of system (2) at E_1 has one negative real eigenvalue $\frac{2k}{k-2}$ and a pair of purely imaginary eigenvalues $\pm\sqrt{gk}i$.

Taking r as the Hopf bifurcation parameter, the transversal condition

$$\mathrm{Re}(\lambda'(r_0))|_{\lambda=\sqrt{gk}i} = \frac{g(2-k)^3}{2k[g(k-2)^2 + 4k]} > 0$$

is also satisfied. Therefore, we have the following theorem:

Theorem 4.2 [Existence of Hopf Bifurcation]. *If $(r, g, m) \in T$ and m varies and passes through the critical value $r_0 = \frac{(m+1)^2}{1-m}$, system (1) undergoes Hopf bifurcations at each equilibrium state $E_{1,2}$.*

The rest of this section is concerned with showing the projection method described in [Sotomayor *et al.*, 2007a, 2007b; Mello & Coelho, 2009] for the calculation of the first Lyapunov coefficient, l_1, associated with the Hopf bifurcation. Consider the differential equation

$$\dot{\overline{X}} = f(\overline{X}, \mu), \tag{5}$$

where $\overline{X} \in \mathbb{R}^3$ and $\mu \in \mathbb{R}^3$ are respectively vectors representing phase space variables and control parameters. Assume that f is in a class of C^∞ in $\mathbb{R}^3 \times \mathbb{R}^3$. Suppose that (5) has an equilibrium point $\overline{X} = X_0$ at $\mu = \mu_0$. Denote the variable $\overline{X} - X_0$ by X and expand

$$F(X) = f(X, \mu_0), \tag{6}$$

as

$$\begin{aligned} F(X) = AX &+ \frac{1}{2}B(X,X) + \frac{1}{6}C(X,X,X) \\ &+ \frac{1}{24}D(X,X,X,X) \\ &+ \frac{1}{120}E(X,X,X,X,X) + O(\|X\|^6), \end{aligned} \tag{7}$$

where $A = f_x(0, \mu_0)$ and, for $i = 1, 2, 3$,

$$B(X,Y) = \sum_{j,k=1}^{3} \frac{\partial^2 F_i(\xi)}{\partial \xi_j \partial \xi_k}\bigg|_{\xi=0} X_j Y_k,$$

$$C(X,Y,Z) = \sum_{j,k,l=1}^{3} \frac{\partial^3 F_i(\xi)}{\partial \xi_j \partial \xi_k \partial \xi_l}\bigg|_{\xi=0} X_j Y_k Z_l,$$

etc., and similar expressions exist for D and E. Suppose that A has a pair of complex eigenvalues on the imaginary axis: $\lambda_{2,3} = \pm i\, w_0$ $(w_0 > 0)$, and these eigenvalues are the only eigenvalues whose real parts are zero. Let T^c be the generalized eigenspace of A corresponding to $\lambda_{2,3}$. Let $p, q \in \mathbb{R}^3$ be vectors such that

$$Aq = iw_0 q, \quad A^T p = -iw_0 p, \quad \langle p, q\rangle = 1, \tag{8}$$

where A^T is the transpose of the matrix A. Any vector $y \in T^c$ can be represented as $y = wq + \overline{w}\overline{q}$, where $w = \langle q, y\rangle \in \mathbb{C}$. The two-dimensional center manifold associated with the eigenvalues $\lambda_{2,3}$ can be parameterized by w and $\overline{w}$, by means of an immersion of the form $X = H(w, \overline{w})$, where $H : \mathbb{C}^2 \to \mathbb{R}^3$ has a Taylor expansion of the form

$$\begin{aligned} H(w,\overline{w}) = wq + \overline{w}\overline{q} &+ \sum_{2\le j+k\le 5} \frac{1}{j!k!} h_{jk} w^j \overline{w}^k \\ &+ O(|w|^6), \end{aligned}$$

with $h_{jk} \in \mathbb{C}^3$ and $h_{jk} = \overline{h}_{kj}$. Substituting this expression into (6) we obtain the differential equation

$$H_w w' + H_w \overline{w}' = F(H(w,\overline{w})),$$

where F is given by (6). The complex vectors h_{ij} are obtained solving the system of linear equations defined by the coefficients of (6), taking into account the coefficients of F, so that system (6), on the chart w for a central manifold, is written as follows

$$\dot{w} = iw_0 w + \frac{1}{2}G_{21} w|w|^2 + \frac{1}{12}G_{32} w|w|^4 + O(|w|^6),$$

where $G_{ij} \in \mathbb{C}$. The first Lyapunov coefficient can be written as

$$l_1 = \frac{1}{2}\operatorname{Re} G_{21}, \tag{9}$$

where $G_{21} = \langle p, C(q,q,\overline{q}) + B(\overline{q}, h_{20}) + 2B(q, h_{11})\rangle$.

4.2. *Hopf bifurcation of system (1)*

In this section, we study the stability of E_1 under the conditions $r = r_0 = \frac{(m+1)^2}{1-m} = \frac{k^2}{2-k}$. Using the notation of the previous section, the multilinear symmetric functions can be written as

$$\begin{aligned} B(X,Y) = (0, &X_1Y_3 + X_3Y_1, 2gmX_1Y_1 \\ &- g(1+m)X_1Y_2 - g(1+m)X_2Y_1), \end{aligned} \tag{10}$$

$$C(X,Y,Z) = (0,0,0). \tag{11}$$

From (8), we have

$$q = \left(\frac{k}{g(-2+k) + 2\sqrt{gk}i}, \frac{-i\sqrt{g}(-2+k) + k^{3/2}}{g(-2+k)\sqrt{k} + 2\sqrt{g}ki}, 1\right),$$

$$p = \left(\frac{1}{2}(-2+k)\sqrt{\frac{g}{k}}i, -\frac{1}{2}\sqrt{gk}i, \frac{1}{2}\right).$$

The complex vectors h_{11} and h_{20} are

$$h_{11} = \left(-\frac{k^2}{g[g(-2+k)^2+4k]}, -\frac{k^2}{g[g(-2+k)^2+4k]}, -\frac{2(-2+k)k}{g(-2+k)^2+4k}\right),$$

$$h_{20} = (h_{201}, h_{202}, h_{203}),$$

where

$$h_{201} = \frac{k^2[3\sqrt{g}(g(-2+k)^2-7k)(-2+k)+2i\sqrt{k}(28g-5k-28gk+7gk^2)]}{3g[\sqrt{g}(-2+k)+i\sqrt{k}]^2[\sqrt{g}(-2+k)+2i\sqrt{k}]^3},$$

$$h_{202} = \frac{\sqrt{k}(-2i\sqrt{g}(-2+k)+k^{(3/2)})(3g(-2+k)^2-10k-22i\sqrt{gk}+11i\sqrt{gk^3})}{3g[\sqrt{g}(-2+k)+i\sqrt{k}][\sqrt{g}(-2+k)+2i\sqrt{k}]^3},$$

$$h_{203} = \frac{2\sqrt{k}(3g^{(3/2)}k^{(5/2)}+12\sqrt{g^3k}-8\sqrt{gk^3}+2igk(-10+5k+6i\sqrt{gk}))}{3[\sqrt{g}(-2+k)+2i\sqrt{k}][g(-2+k)+2i\sqrt{gk}]^2}.$$

The complex coefficient G_{21} defined in (5) takes the form

$$G_{21} = -\frac{2k^{5/2}[3ig(-2+k)^2-4ik+12\sqrt{gk}-6\sqrt{gk^3}]}{3\sqrt{g}[g(-2+k)^2+4k][g(-2+k)^2-6i\sqrt{gk}+k(-2+3i\sqrt{gk})]}.$$

We then have the following theorem:

Theorem 4.3. *Consider system (1) with $r > 0$, $g > 0$, $0 < m < 1$. The first Lyapunov coefficient associated with the equilibria $E_{1,2}$ is given by*

$$l_1 = \frac{1}{2}\operatorname{Re} G_{21} = \frac{2g(1+m)^3(1-3m+3m^2-m^3)}{[1+g(-1+m)^2+m][(g(-1+m)^2+4(1+m)]^2} > 0. \tag{12}$$

Then the equilibria $E_{1,2}$ of the three-parameter family of differential equations (1) undergo a transversal Hopf bifurcation when $r = r_0 = \frac{(m+1)^2}{1-m}$. More specifically, when $r < r_0$, but near to r_0, there exist two unstable limit cycles around the asymptotically stable equilibria $E_{1,2}$.

The sign of the first Lyapunov coefficient is determined by the sign of the numerator of (12) since the denominator is positive. Observe that the first Lyapunov coefficient is positive, which means there are no degenerate Hopf bifurcation. In addition, what is interesting is to further find out the kind of dynamical behaviors system (1) has at infinity when $m > -1$, $m = -1$, or $m < -1$, which is the main focus of the report in Sec. 6.

4.3. *Hidden attractors and numerical simulations*

In this section, we present some numerical simulations of system (1) for several values of the parameters. The main purpose is to illustrate the creation of unstable limit cycles through the Hopf bifurcations at the equilibria $E_{1,2}$ (proved to occur in the previous subsections), and to demonstrate the existence of the hidden chaotic attractor.

For $g = 20$ and $m = 0.75$, system (1) has two stable equilibria when $r < 12.25$. Note that for these parameter values, we have the Hopf bifurcation value $r_0 = 12.25$. According to Theorem 4.3, system (1) undergoes a Hopf bifurcation when the parameter r crosses the critical value $r = r_0$, and two unstable periodic orbits emerge from E_1 and E_2 with $r < r_0$ and r near r_0, respectively. Choosing initial values $(1, 1.05, 1.75)$ near the equilibrium E_1, we take $r = 12.145 < r_0$, and an unstable periodic orbit exists near the stable equilibrium E_1. Similarly, there is also an unstable periodic orbit existing with initial conditions $(-1, -1.05, 1.75)$ near the stable equilibrium E_2. Furthermore, when the initial value moves away from the above two sets, hidden chaotic attractors emerge from the unstable periodic orbits that arose in the Hopf bifurcation.

We can conclude that unstable periodic solutions can be found near the stable equilibria point $E_{1,2}$ for $r < r_0$. This unstable periodic solution leads to the generation of hidden chaotic attractors. All results can be displayed in Fig. 6.

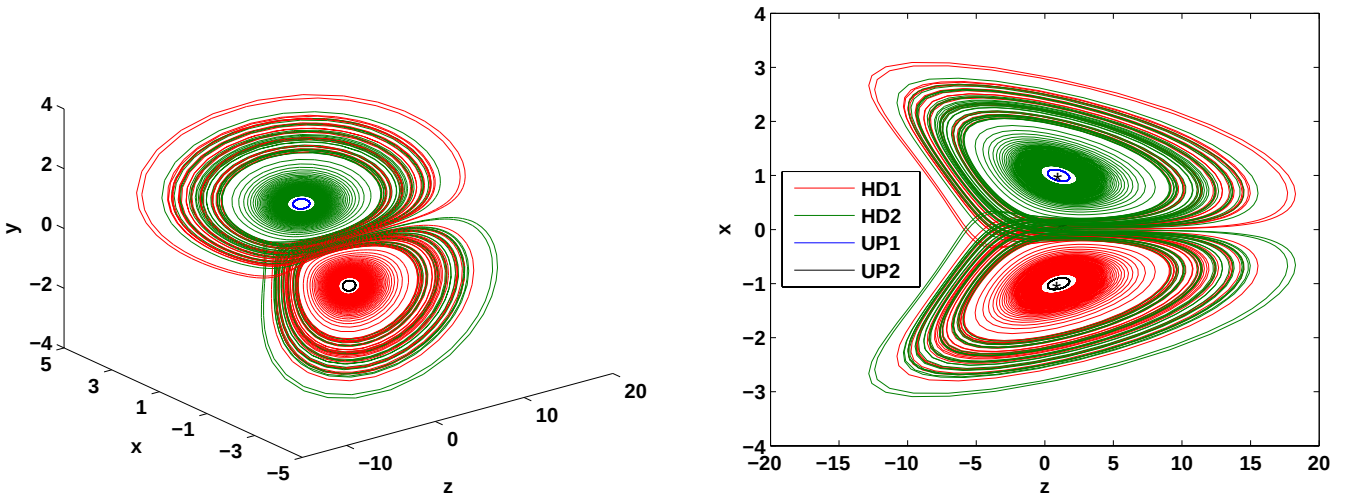

(a) (b)

Fig. 6. Phase diagrams of the system (1) versus parameters $(r, m, g) = (12.145, 0.75, 20)$. Red orbit means hidden chaotic attractor (HD1) with initial values $(-1.2, -1.2, 1.2)$ near stable equilibrium E_2 $(-1, -1, 1)$; Green orbit means hidden chaotic attractor (HD2) with initial values $(1.2, 1.2, 1.2)$ near stable equilibrium E_1 $(1, 1, 1)$; Blue orbit means unstable periodic solution (UP1) with initial values $(1, 1.05, 1.75)$ near stable equilibrium E_1 $(1, 1, 1)$ from Hopf bifurcation; Black orbit means unstable periodic solution (UP2) with initial values $(-1, -1.05, 1.75)$ near stable equilibrium E_2 $(-1, -1, 1)$ from Hopf bifurcation.

4.4. *Unstable periodic orbits*

The chaotic attractor can be thought of as a concatenation of unstable periodic orbits (upos) of different periods. We are able to extract such orbits by constructing a Poincaré section through the z equilibrium value of $z = 1$, following the method of Hénon [1982].

If we introduce a new variable $Z = z - 1$, then the revised equilibrium states become $(x, y, Z) = (\pm 1, \pm 1, 0)$, and we take the Poincaré section as

$$\mathcal{S} = \{(x, y) : Z = 0, \dot{Z} > 0, x > 0\}.$$

In order to extract the upos, we integrated system (1) for 60 000 time units with a time step of 0.001 sec, discarded the first 100 sec as representing transients. The criterion for choosing close returns on the Poincaré section $\mathcal{S}$ was:

$$\|\mathbf{Z}_i - \mathbf{Z}_j\| < \epsilon,$$

where $\mathbf{Z}_h = (x_h, y_h, Z_h)$ and $h = i, j$ are the ith and jth intersections on $\mathcal{S}$. We chose both $\epsilon = 0.005$ and $\epsilon = 0.001$ to compare the histograms of unstable periodic orbits, and to select typical examples of upos of lowest period. By following the method of Hénon [1982], we can ensure that the trajectories land precisely on the Poincaré section by rewriting (1) with Z as the independent variable, instead of t. We then integrate the revised system for one step from Z_η to $Z = 0$, where t_η is the time just before Z changes sign.

Because of the reflectional symmetry of system (1), if (x, y, z) is a trajectory, then so is $(-x, -y, z)$. Figure 7 shows the phase portraits of three of the lowest order upos, together with a plot of the hidden attractor on which these upos are inserted. We label the orbits from a knowledge of their individual time series as follows. If the trajectory falls in $x > 0$, we label that part symbolically as R, while if the trajectory falls in $x < 0$, we label it as L. We show each of the three upos in a different color, so that they are easily identifiable on the hidden attractor, shown in Fig. 7(d).

Here $R^p L^q$ means the trajectory oscillates p times around the $(x, y) = (1, 1)$ equilibrium state, before oscillating q times around the $(x, y) = (-1, -1)$ state. Figure 7(a) shows an example of an RL upo of period 2.855 sec in blue, while Fig. 7(b) shows an R^2L^2 upo of period 6.55 sec in red. Figure 7(c) shows an $RLRL^2$ upo with period 6.884 sec in black. Finally in Fig. 7(d), we show these three orbits are placed on the hidden attractor. The yellow trajectories correspond to initial conditions $(x, y, z) = (1.2, 1.2, 1.2)$, while the green trajectories correspond to initial conditions $(x, y, z) = (-1.2, -1.2, 1.2)$.

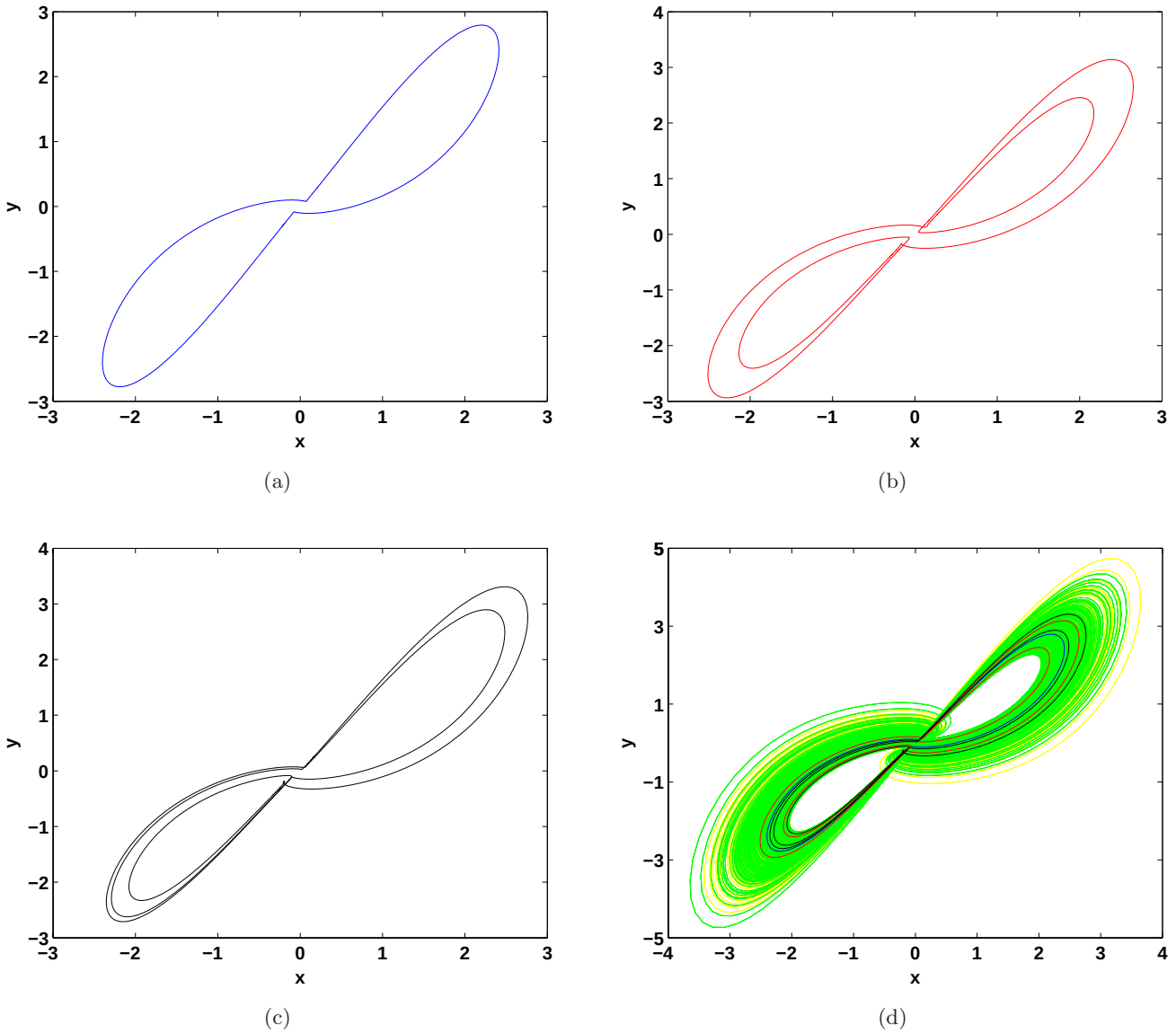

Fig. 7. The phase portraits of three upos of system (1) in the (x, y)-planes, together with their locations on the hidden chaotic attractor. Specifically (a) shows an RL upo with period 2.855 sec, (b) shows an R^2L^2 upo of period 6.55 sec, (c) shows an $RLRL^2$ upo with period 6.884 sec and (d) shows the hidden attractor and its reflectionally symmetric partner, together with the three upos of (a)–(c).

5. Existence of Homoclinic Orbits

In order to analyze the existence of homoclinic orbits of system (5), we introduce the generalized Melnikov method developed by Wiggins and Holmes [1987, 1988].

Consider the following system:

$$\begin{cases} \dot{x} = f_1(x.y, z) + \varepsilon g_1(x, y, z), \\ \dot{y} = f_2(x.y, z) + \varepsilon g_2(x, y, z), \\ \dot{z} = \varepsilon g_3(x, y, z), \end{cases} \tag{13}$$

where $0 < \varepsilon \ll 1$, and $f_i(x \cdot y, z)$ $(i = 1, 2)$, $g_i(x \cdot y, z)$ $(i = 1, 2, 3)$ are sufficiently smooth functions. We make the following assumptions on the unperturbed system when $\varepsilon = 0$:

Assumption H1. System $(13)_{\varepsilon=0}$ is a one-parameter family of planar Hamiltonian systems with Hamiltonian function $H(x, y, z)$,

$$\begin{cases} \dot{x} = f_1(x.y, z) = \dfrac{\partial H}{\partial y}, \\ \dot{y} = f_2(x.y, z) = -\dfrac{\partial H}{\partial x}, \\ \dot{z} = 0. \end{cases} \tag{14}$$

Assumption H2. For each value of z in some open interval $J \subset \mathbb{R}$, (14) has a one-parameter family of periodic orbits, $q^{\alpha,z}(t)$, $\alpha \subset L(z) \subset \mathbb{R}$, with a homoclinic orbit $q^{\alpha_0}(t)$ to a hyperbolic saddle point $\gamma(z) = (x(z), y(z))$. Let $T(\alpha, z)$ be the period of $q^{\alpha,z}(t)$. Assume that $\lim_{\alpha\to\alpha_0} T(\alpha, z) = \infty$, $dT(\alpha, z)/d\alpha \neq 0$ for $(\alpha, z) \in (L(z), J)$, where $L(z)$ is an open interval in $\mathbb{R}$.

Writing the scalar Melnikov function for the existence of homoclinic orbits

$$M_0(z) = \int_{-\infty}^{+\infty} \left(f_1 g_2 - f_2 g_1 + \frac{\partial H}{\partial z} g_3\right)(q^{\alpha_0,z}(t), z)dt - \frac{\partial H}{\partial z}(\gamma(z), z) \int_{-\infty}^{+\infty} g_3(q^{\alpha_0,z}(t), z)dt. \tag{15}$$

Then the following results in [Wiggins & Holmes, 1988] hold.

Lemma 5.1. *Suppose that the homoclinic orbit of $(13)_\varepsilon$ depends on a scalar parameter $z \in K \subseteq \mathbb{R}$ and there exists a point $z_0 \in K$ such that*

$$M_0(z_0) = 0, \quad \left.\frac{\partial M_0(z)}{\partial z}\right|_{z=z_0} \neq 0. \tag{16}$$

Then for $\varepsilon \neq 0$ sufficiently small, there exists a nontransverse homoclinic orbit of $(13)_\varepsilon$ near μ_0.

Under the transformation $z \to z - m$, system (1) becomes

$$\begin{cases} \dot{x} = r(y - x) \\ \dot{y} = -(1 + m)y + xz \\ \dot{z} = g + gmx^2 - g(1 + m)xy. \end{cases} \tag{17}$$

Introducing the rescaling:

$$x \to \frac{rx}{\varepsilon\sqrt{g(1+m)}}, \quad y \to -\frac{ry}{\varepsilon^2\sqrt{g(1+m)}},$$
$$z \to \frac{rz}{\varepsilon^2}, \quad t \to \frac{\varepsilon t}{r}, \quad \varepsilon = \frac{1}{\sqrt{g}},$$

system (17) becomes

$$\begin{cases} \dot{x} = -y - \varepsilon x, \\ \dot{y} = -xz - \varepsilon\dfrac{1+m}{r}y, \\ \dot{z} = xy + \varepsilon\left(\dfrac{m}{1+m}x^2 + \dfrac{1}{r^2}\right). \end{cases} \tag{18}$$

Therefore, we only need to establish the existence of homoclinic orbits in system (18).

When $\varepsilon = 0$, system (18) can be seen as a three-dimensional generalized Hamiltonian system

$$\frac{d}{dt}\begin{pmatrix} x \\ y \\ z \end{pmatrix} = \begin{pmatrix} 0 & 0 & -y \\ -z & 0 & 0 \\ y & 0 & 0 \end{pmatrix}\begin{pmatrix} x \\ 0 \\ 1 \end{pmatrix} = J\begin{pmatrix} \dfrac{\partial H}{\partial x} \\ \dfrac{\partial H}{\partial y} \\ \dfrac{\partial H}{\partial z} \end{pmatrix},$$

with Hamiltonian function

$$H(x, y, z) = z + \frac{x^2}{2} = A \tag{19}$$

and Casimir function

$$C(x, y, z) = y^2 + z^2 = \rho^2.$$

Let $\rho > 0$ and make a polar-coordinate transformation

$$\begin{cases} x = x, \\ y = \rho\cos\left(\theta - \dfrac{\pi}{2}\right), \\ z = \rho\sin\left(\theta - \dfrac{\pi}{2}\right), \end{cases} \tag{20}$$

then (18) becomes

$$\begin{cases} \dot{\rho} = -\varepsilon\left[\rho\dfrac{1+m}{r}\sin^2\theta + \cos\theta\left(\dfrac{m}{1+m}x^2 + \dfrac{1}{r^2}\right)\right], \\ \dot{\theta} = x + \varepsilon\left[\dfrac{\sin\theta}{\rho}\left(\dfrac{m}{1+m}x^2 + \dfrac{1}{r^2}\right) + \dfrac{1+m}{r}\sin\theta\cos\theta\right], \\ \dot{x} = -\rho\sin\theta - \varepsilon x. \end{cases} \tag{21}$$

The following result can then be obtained.

Theorem 5.2. *Let $5(3 - m)r - 3(1 + m)^2 > 0$. Then, for ε sufficiently small near the two homoclinic orbits $\Gamma_{h_\pm}$ of system $(21)_{\varepsilon=0}$, system (21) possesses two nontransverse homoclinic orbits near*

$$y^2 + z^2 = \rho_*^2,$$

where

$$\rho_* = \frac{15(1+m)}{2r[5(3-m)r - 3(1+m)^2]}.$$

Proof. According to (19) and (20), system $(21)_\varepsilon = 0$ is Hamiltonian system with Hamiltonian function $H(x, r, \theta)$ given by

$$H(x, r, \theta) = \frac{x^2}{2} - \rho\cos\theta = A.$$

Therefore, it is easy to find that, when $A = \rho$, there are two homoclinic orbits $\Gamma^1_{h_\pm}$ of $(21)_{\varepsilon=0}$ connecting the saddle point $(\rho, \pi, 0)$, whose parametric expressions

$$\begin{cases} \theta_h(t) = \pm 2\arctan(\sinh\sqrt{\rho}t), \\ x_h(t) = \pm 2\sqrt{\rho}(\operatorname{sech}\sqrt{\rho}t). \end{cases} \tag{22}$$

By mean of (21) and (22), the Melnikov function

$$\begin{aligned} M(\rho) &= \int_{-\infty}^{+\infty} \left[-x_h^2(t) + \sin^2\theta_h(t)\left(\frac{m}{1+m}x^2 + \frac{1}{r^2}\right) + \rho\sin^2\theta_h(t)\cos\theta_h(t)\frac{1+m}{r}\right] dt \\ &\quad + \int_{-\infty}^{+\infty} \cos\theta_h(t)\left[\rho\frac{1+m}{r}\sin^2\theta + \cos\theta\left(\frac{m}{1+m}x^2 + \frac{1}{r^2}\right)\right] dt \\ &\quad + \int_{-\infty}^{+\infty} \left[\rho\frac{1+m}{r}\sin^2\theta + \cos\theta\left(\frac{m}{1+m}x^2 + \frac{1}{r^2}\right)\right] dt \\ &= \frac{4}{r^2\sqrt{\rho}} + \frac{8m\sqrt{\rho}}{3(1+m)} - \frac{8}{1+m}\sqrt{\rho} + \frac{8(1+m)\sqrt{\rho}}{5r}, \end{aligned}$$

implies that

$$M(\rho_*) = 0, \quad \left.\frac{\partial M}{\partial\rho}\right|_{\rho=\rho_*} \neq 0,$$

when

$$\rho = \rho_* = \frac{15(1+m)}{2r[5(3-m)r - 3(1+m)^2]},$$

where $5(3-m)r - 3(1+m)^2 > 0$. Therefore, by using Lemma 5.1, for ε sufficiently small near the two homoclinic orbits $\Gamma^1_{h_\pm}$ of system $(21)_{\varepsilon=0}$, it possesses two nontransverse homoclinic orbits. From (18), (20) and (21), it follows that the conclusion in Theorem 5.2 hold. ■

6. Infinity Dynamics by Poincaré Compactification

Although the physical relevance of m in Sec. 2 has $m > 0$, for mathematical completeness we explore the whole range of possible values for m. In order to study the behavior of the trajectories of the system (1) near infinity, we will use the theory of Poincaré compactification in R^3 [Cima & Llibre, 1990; Llibre & Messias, 2009; Llibre *et al.*, 2012]. Let the Poincaré ball $S^3 = \{\gamma = (\gamma_1, \gamma_2, \gamma_3, \gamma_4) \in R^4 \,|\, \|\gamma\| = 1\}$ be the unit sphere, $S_+ = \{\gamma \in S^3, \gamma_4 > 0\}$ and $S_- = \{\gamma \in S^3, \gamma_4 < 0\}$ be the northern and southern hemispheres, denote the tangent hyperplanes at the point $(\pm1, 0, 0, 0)$, $(0, \pm1, 0, 0)$, $(0, 0, \pm1, 0)$, $(0, 0, 0, \pm1)$ by the charts U_i, V_i for $i = 1, 2, 3, 4$, where $U_i = \{\gamma \in S^3, \gamma_i > 0\}$, $V_i = \{\gamma \in S^3, \gamma_i < 0\}$. We only consider the chart U_i, V_i for $i = 1, 2, 3$ for getting the dynamics at x, y, z infinity.

In the charts U_1 and V_1

With the change of variables $(x, y, z) = (w^{-1}, uw^{-1}, vw^{-1})$, and $t = w\tau$, the system (1) becomes

$$\begin{cases} \dfrac{du}{d\tau} = -ru^2w - muw \to +ruw + mw - uw + v, \\ \dfrac{dv}{d\tau} = -ruvw - gmu + gw^2 + rvw + gm - gu, \\ \dfrac{dw}{d\tau} = -ruw^2 + rw^2. \end{cases} \tag{23}$$

If $w = 0$, system (23) reduces to

$$\begin{cases} \dfrac{du}{d\tau} = v, \\ \dfrac{dv}{d\tau} = -gmu + gm - gu. \end{cases} \tag{24}$$

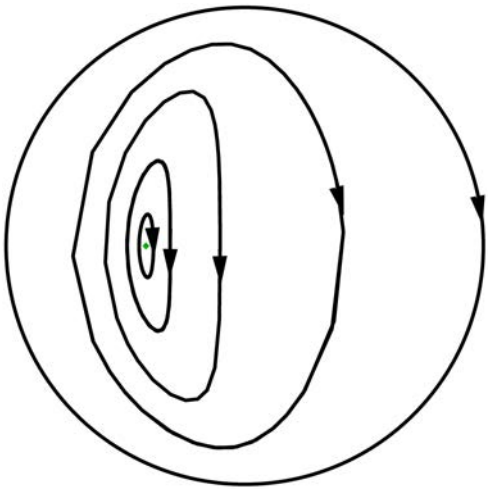

Fig. 8. Trajectories in the global phase portraits of system (24) for $m > -1$.

Clearly, we can see that (24) is a Hamiltonian system with the Hamiltonian function as

$$H = \frac{1}{2}v^2 + \frac{1}{2}g(m+1)u^2 - gmu.$$

When $m > -1$ the system (24) has a center, and has a saddle when $m < -1$ or has a parabolic orbit when $m = -1$. The corresponding global phase portraits of Eq. (24) are shown in Figs. 8–10.

The flow in the chart V_1 is the same as the flow in the chart U_1 reversing time. Hence, the phase portrait of system (1) on the infinite sphere at the negative end point of the x-axis is shown in Figs. 8–10, reversing the time direction.

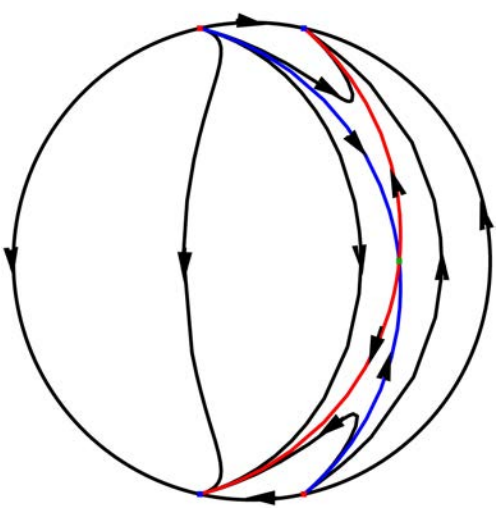

Fig. 9. Trajectories in the global phase portraits of system (24) for $m < -1$.

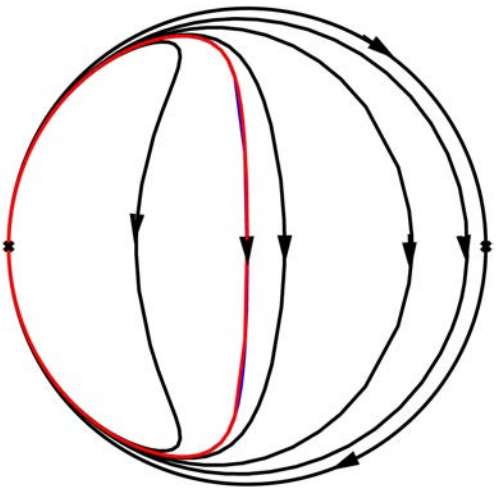

Fig. 10. Trajectories in the global phase portraits of system (24) for $m = -1$.

In the charts U_2 and V_2

Next, we study the dynamics of the system (1) at infinity of the y-axis. Taking the transformation $(x, y, z) = (uw^{-1}, w^{-1}, vw^{-1})$, and $t = w\tau$, the system (1) becomes

$$\begin{cases} \dfrac{du}{d\tau} = -mu^2w + muw - ruw - u^2v + rw + uw, \\ \dfrac{dv}{d\tau} = gmu^2 - muvw - gmu + gw^2 \\ \qquad\qquad + mvw - uv^2 - gu + vw, \\ \dfrac{dw}{d\tau} = -muw^2 + mw^2 - uvw + w^2. \end{cases} \tag{25}$$

If $w = 0$, system (25) reduces to

$$\begin{cases} \dfrac{du}{d\tau} = -u^2v, \\ \dfrac{dv}{d\tau} = gmu^2 - gmu - uv^2 - gu. \end{cases} \tag{26}$$

Clearly, the system (26) has a line of equilibrium points $u = 0$. When $m > -1$ system (26) has a center, it also has a saddle and two nodes when $m < -1$ or has homoclinic loops when $m = -1$. The corresponding global phase portraits of Eq. (26) are shown in Figs. 11–13.

The flow in the chart V_2 is the same as the flow in the local chart U_2. Hence, the phase portrait of system (1) on the infinite sphere at the negative end

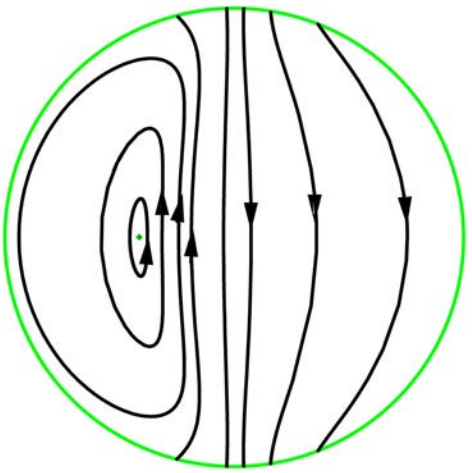

Fig. 11. Trajectories in the global phase portraits of system (26) for $m > -1$.

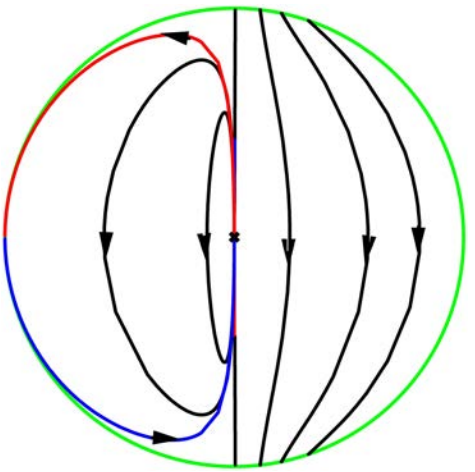

Fig. 13. Trajectories in the global phase portraits of system (26) for $m = -1$.

point of the y-axis is shown in Figs. 11–13, reversing the time direction.

In the charts U_3 and V_3

Finally, we consider infinity along the z-axis. Let $(x, y, z) = (uw^{-1}, vw^{-1}, w^{-1})$, and $t = w\tau$, the system (1) becomes

$$\begin{cases} \dfrac{du}{d\tau} = -gmu^3 + gmu^2 + gu^2v \\ \qquad\quad - guw^2 - ruw + rvw, \\ \dfrac{dv}{d\tau} = -gmu^2v + gmuv^2 + guv^2 - gvw^2 \\ \qquad\quad + muw - mvw - vw + u, \\ \dfrac{dw}{d\tau} = -gmu^2w + gmuvw + guvw - gw^3. \end{cases} \tag{27}$$

If $w = 0$, system (27) reduces to

$$\begin{cases} \dfrac{du}{d\tau} = -gmu^3 + gmu^2v + gu^2v, \\ \dfrac{dv}{d\tau} = -gmu^2v + gmuv^2 + guv^2 + u. \end{cases} \tag{28}$$

Clearly, system (28) has a line of equilibrium points $u = 0$. Furthermore, when $m > -1$, system (28) has no equilibrium points. When $m < -1$, system (28) has heteroclinic loops which connected the equilibrium points $(0, \pm\frac{1}{\sqrt{-g(m+1)}})$. When $m = -1$, system (28) has parabolic orbits. The corresponding global phase portraits of Eq. (26) are as shown in Figs. 14–16.

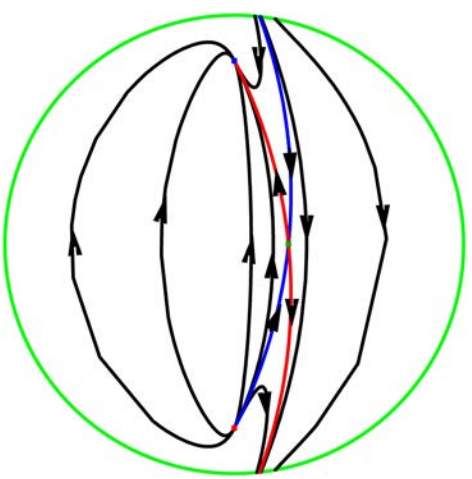

Fig. 12. Trajectories in the global phase portraits of system (26) for $m < -1$.

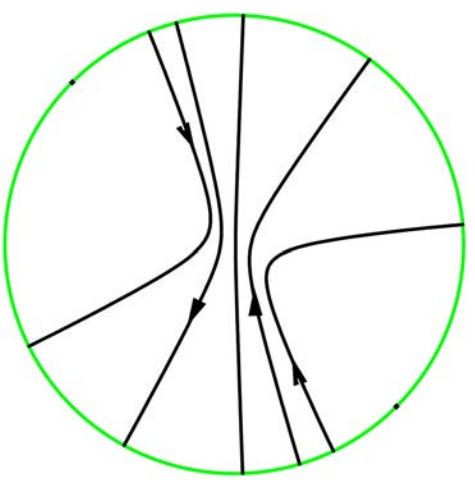

Fig. 14. Trajectories in the local phase portraits of system (28) for $m > -1$.

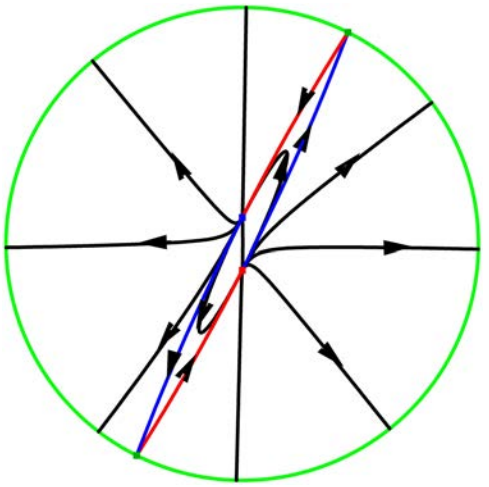

Fig. 15. Trajectories in the local phase portraits of system (28) for $m < -1$.

The flow in the chart V_3 is the same as the flow in the local chart U_3. Hence, the phase portrait of system (1) on the infinite sphere at the negative end point of the z-axis is shown in Figs. 14–16, reversing the time direction. Therefore, we can make the following remark about dynamics at infinity on the Poincaré sphere.

Remark 6.1. The phase portrait of system (1) on the Poincaré sphere at infinity is as shown in Figs. 17–19. There exist two centers at the front hemisphere and the back hemisphere for $m > -1$, two saddles at the left hemisphere and the right hemisphere for $m < -1$, and homoclinic loops at the front hemisphere and the back hemisphere for $m = -1$.

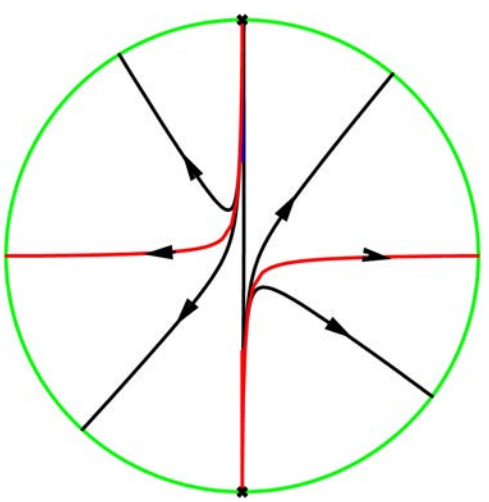

Fig. 16. Trajectories in the local phase portraits of system (28) for $m = -1$.

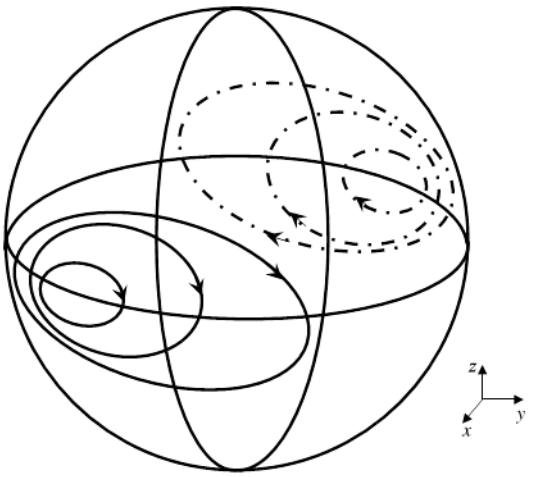

Fig. 17. Phase portrait of the system (1) on the Poincaré sphere at infinity for $m > -1$.

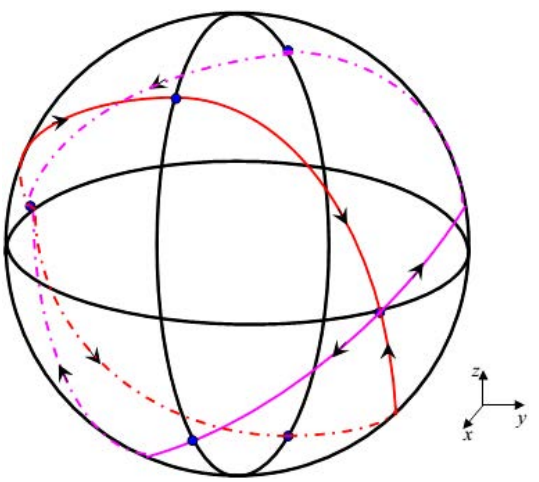

Fig. 18. Phase portrait of the system (1) on the Poincaré sphere at infinity for $m < -1$.

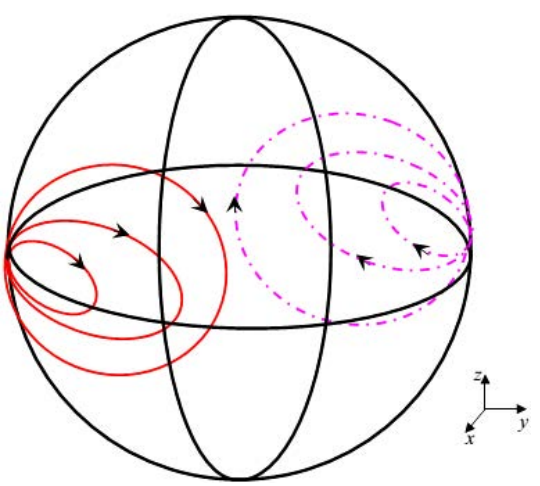

Fig. 19. Phase portrait of the system (1) on the Poincaré sphere at infinity for $m = -1$.

7. Conclusion

One key result of the work reported in this paper is to show hidden chaotic attractors throughout the parameter region which only admits stable equilibria in the segmented disc dynamo, known as Moffatt system [Moffatt, 1979]. In contrast we found hidden chaotic solutions to occur well away from the subcritical Hopf bifurcation, which will have potential applications in the field of disc dynamos.

We also discussed the mechanisms responsible for the particular dynamics and provided an overview of various 2D parameter spaces. The hidden chaos of the Moffatt system has been analyzed in detail, through discussions of the Hopf bifurcation. Moreover, we proved that the Moffatt system possesses homoclinic orbits, which implies a possible mechanism causing chaotic dynamics. By using the Poincaré compactification for polynomial vector fields in R^3, we studied the dynamics of the Moffatt system at infinity. In this sense, since the dynamics are very sensitive to initial conditions it does not seem that a numerical approach would allow us to understand how the solutions reach infinity when $t \to \infty$.

Another form of complexity arises when two or more asymptotically stable equilibrium points or attracting sets coexist as the Moffatt system parameters are being varied. This is usually referred to as coexisting attractors and when this occurs, the trajectories of the system selectively converge on either of the attracting sets depending on the initial state of the system. When coexisting attractors occur, engineers and scientists are usually interested in obtaining the basins of attraction of the different attracting sets, defined as the set of initial points whose trajectories converge on the given attractor [Dudkowski *et al.*, 2016].

Acknowledgments

We would like to express our gratitude to Prof. H. K. Moffatt for his encouraging comments. We thank the Mathematical Institute, University of Oxford for providing the facilities and the China Scholarship Council (No. 201506415023). This work was supported by the Open Foundation for Guangxi Colleges and Universities Key Lab of Complex System Optimization and Big Data Processing (No. 2016CSOBDP0202), the Natural Science Foundation of China (No. 11401543), Beijing Postdoctoral Research Foundation (No. 2015ZZ17), the China Postdoctoral Science Foundation funded project (Nos. 2014M560028 and 2015T80029), the Fundamental Research Funds for the Central Universities, China University of Geosciences (Wuhan) (No. CUGL150419), the Natural Science Foundation of Hubei Province (No. 2014CFB897), the Government of Chaoyang District Postdoctoral Research Foundation (No. 2015ZZ-7), and the Funding Project for Academic Human Resources Development in Institutions of Higher Learning under the Jurisdiction of Beijing Municipality (PHRIHLB).

References

Andrievsky, B. R., Kuznetsov, N. V., Leonov, G. A. & Pogromsky, A. Y. [2013] "Hidden oscillations in aircraft flight control system with input saturation," *IFAC-PapersOnline* **5**, 75–79.

Beck, R., Brandenburg, A., Moss, D., Shukurov, A. & Sokolov, D. [1996] "Galactic magnetism: Recent developments and perspectives," *Ann. Rev. Astron. Astrophys.* **34**, 155–206.

Blekhman, I., Indeitsev, D. & Fradkov, A. [2007] "Slow motions in systems with inertially excited vibrations," *IFAC-PapersOnline* **3**, 126–131.

Bullard, E. C. [1955] "The stability of a homopolar dynamo," *Proc. Camb. Phil. Soc.* **51**, 744–760.

Cima, A. & Llibre, J. [1990] "Bounded polynomial vector fields," *Trans. Amer. Math. Soc.* **318**, 557–579.

Dudkowski, D., Jafari, S., Kapitaniak, T., Kuznetsov, N. V., Leonov, G. A. & Prasad, A. [2016] "Hidden attractors in dynamical systems," *Phys. Rep.* **637**, 1–50.

Eckert, M. & Sommerfeld, A. [2013] *Science, Life and Turbulent Times* (Springer-Verlag, NY), pp. 1868–1951.

Hénon, M. [1982] "On the numerical computation of Poincaré maps," *Physica D* **5**, 412–414.

Hide, R., Skeldon, A. C. & Acheson, D. J. [1996] "A study of two novel self-exciting single-disk homopolar dynamos: Theory," *Proc. Roy. Soc. Lond. A* **452**, 1369–1395.

Hilbert, D. [1901] "Mathematical problems," *Bull. Amer. Math. Soc.* **8**, 437–479.

Jafari, S., Sprott, J. C. & Golpayegani, S. M. R. H. [2013] "Elementary quadric chaotic flows with no equilibria," *Phys. Lett. A* **377**, 699–702.

Kiseleva, M. A., Kuznetsov, N. V. & Leonov, G. A. [2016] "Hidden attractors in electromechanical systems with and without equilibria," *IFAC-PapersOnLine* **49**, 51–55.

Knobloch, E. [1981] "Chaos in the segmented disc dynamo," *Phys. Lett. A* **82**, 439–440.

Kuznetsov, Y. A. [2014] *Elements of Applied Bifurcation Theory* (Springer-Verlag, NY).

Kuznetsov, N. V., Mokaev, T. N. & Vasilyev, P. A. [2014] "Numerical justification of Leonov conjecture on Lyapunov dimension of Rössler attractor," *Commun. Nonlin. Sci. Numer. Simulat.* **19**, 1027–1034.

Kuznetsov, A. P., Kuznetsov, S. P., Mosekilde, E. & Stankevich, N. V. [2015] "Co-existing hidden attractors in a radio-physical oscillator system," *J. Phys. A: Math. Theor.* **48**, 125101.

Kuznetsov, N. V. [2016] "The Lyapunov dimension and its estimation via the Leonov method," *Phys. Lett. A* **380**, 2142–2149.

Kuznetsov, N. V., Leonov, G. A., Mokaev, T. N. & Seledzhi, S. M. [2016] "Hidden attractor in the Rabinovich system, Chua circuits and PLL," *AIP Conf. Proc.* **1738**, 210008.

Leonov, G. A., Kuznetsov, N. V. & Vagaitsev, V. I. [2012] "Hidden attractor in smooth Chua systems," *Physica D* **241**, 1482–1486.

Leonov, G. A. & Kuznetsov, N. V. [2013] "Hidden attractors in dynamical systems: From hidden oscillation in Hilbert–Kolmogorov, Aizerman and Kalman problems to hidden chaotic attractor in Chua circuits," *Int. J. Bifurcation and Chaos* **23**, 1330002-1–.

Leonov, G. A., Kuznetsov, N. V., Yuldashev, M. & Yuldashev, R. [2014] "Nonlinear analysis of classical phase-locked loops in signal's phase space," *IFAC-PapersOnLine* **19**, 8253–8258.

Leonov, G. A., Kuznetsov, N. V. & Mokaev, T. N. [2015a] "Homoclinic orbits, and self-excited and hidden attractors in a Lorenz-like system describing convective fluid motion," *Eur. Phys. J. Spec. Top.* **224**, 1421–1458.

Leonov, G. A., Kuznetsov, N. V. & Mokaev, T. N. [2015b] "Homoclinic orbit and hidden attractor in the Lorenz-like system describing the fluid convection motion in the rotating cavity," *Commun. Nonlin. Sci. Numer. Simulat.* **28**, 166–174.

Llibre, J. & Messias, M. [2009] "Global dynamics of the Rikitake system," *Physica D* **238**, 241–252.

Llibre, J., Messias, M. & Silva, P. R. Da. [2012] "Global dynamics in the Poincaré ball of the Chen system having invariant algebraic surfaces," *Int. J. Bifurcation and Chaos* **22**, 1250154-1–17.

Mello, L. F. & Coelho, S. F. [2009] "Degenerate Hopf bifurcations in the Lü system," *Phys. Lett. A* **373**, 1116–1120.

Moffatt, H. K. [1978] *Magnetic Field Generation in Electrically Conducting Fluids* (Cambridge Univ. Press).

Moffatt, H. K. [1979] "A self consistent treatment of simple dynamo systems," *Geophys. Astrophys. Fluid Dyn.* **14**, 147–166.

Moroz, I. M., Hide, R. & Soward, A. M. [1998] "On self-exciting coupled Faraday disk homopolar dynamos driving series motors," *Physica D* **117**, 128–144.

Priede, J. & Avalos-Zúñiga, R. [2013] "Feasible homopolar dynamo with sliding liquid-metal contacts," *Phys. Lett. A* **377**, 34–36.

Shilnikov, L. P. [1965] "A case of the existence of a denumerable set of periodic motions," *Sov. Math. Dokl.* **6**, 163–166.

Silva, C. P. [1993] "Shilnikov's theorem-a tutorial," *IEEE Trans. Circuits Syst.-I* **40**, 657–682.

Sommerfeld, A. [1902] "Beitrage zum dynamischen ausbau der festigkeitslehre," *Z. Vereins Deutscher Ingenieure* **46**, 391–394.

Sotomayor, S., Mello, L. F. & Braga, D. C. [2007a] "Bifurcation analysis of the Watt governor system," *Commun. Appl. Math.* **26**, 19–44.

Sotomayor, S., Mello, L. F. & Braga, D. C. [2007b] "Lyapunov coefficients for degenerate Hopf bifurcations," arXiv:0709.3949v1 [math.DS], http://arxiv.org/.

Wang, X. & Chen, G. R. [2012] "A chaotic system with only one stable equilibrium," *Commun. Nonlin. Sci. Numer. Simulat.* **17**, 1264–1272.

Wang, Z., Cang, S., Ochola, E. O. & Sun, Y. [2012] "A hyperchaotic system without equilibrium," *Nonlin. Dyn.* **69**, 531–537.

Wang, X. & Chen, G. R. [2013] "Constructing a chaotic system with any number of equilibria," *Nonlin. Dyn.* **71**, 429–436.

Wei, Z. C. [2011] "Dynamical behaviors of a chaotic system with no equilibria," *Phys. Lett. A* **376**, 102–108.

Wei, Z. C. & Yang, Q. G. [2011] "Dynamical analysis of a new autonomous 3D chaotic system only with stable equilibria," *Nonlin. Anal.: Real World Appl.* **12**, 106–118.

Wei, Z. C. & Yang, Q. G. [2012] "Dynamical analysis of the generalized Sprott C system with only two stable equilibria," *Nonlin. Dyn.* **68**, 543–554.

Wei, Z. C., Sprott, J. C. & Chen, H. [2015a] "Elementary quadratic chaotic flows with a single non-hyperbolic equilibrium," *Phys. Lett. A* **379**, 2184–2187.

Wei, Z. C., Zhang, W., Wang, Z. & Yao, M. H. [2015b] "Hidden attractors and dynamical behaviors in an extended Rikitake system," *Int. J. Bifurcation and Chaos* **25**, 1550028-1–11.

Wei, Z. C., Moroz, I., Wang, Z., Sprott, J. C. & Kapitaniak, T. [2016] "Dynamics at infinity, degenerate Hopf and zero-Hopf bifurcation for Kingni–Jafari system with hidden attractors," *Int. J. Bifurcation and Chaos* **26**, 1650125-1–16.

Wiggins, S. & Holmes, P. [1987] "Homoclinic orbits in slowly varying oscillators," *SIAM J. Math. Anal.* **18**, 612–629.

Wiggins, S. & Holmes, P. [1988] "Homoclinic orbits in slowly varying oscillators," *SIAM J. Math. Anal.* **19**, 1254–1255, Erratum.

Zhusubaliyev, Z. T., Mosekilde, E., Churilov, A. N. & Medvedev, A. [2015] "Multistability and hidden attractors in an impulsive Goodwin oscillator with time delay," *Eur. Phys. J. Spec. Top.* **224**, 1519–1539.